

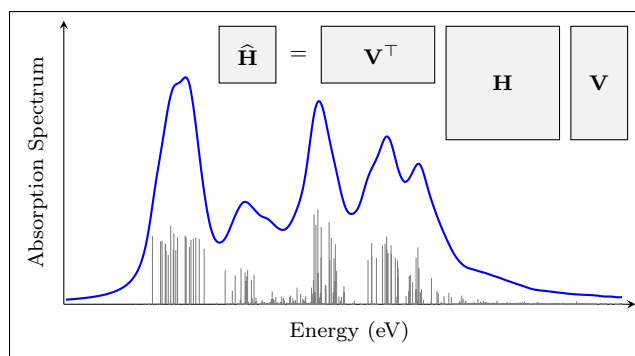
A Model Order Reduction Algorithm for Estimating the Absorption Spectrum

Roel Van Beeumen,^{*,†} David B. Williams-Young,^{*,‡} Joseph M. Kasper,^{*,‡} Chao
Yang,^{*,†} Esmond G. Ng,^{*,†} and Xiaosong Li^{*,‡}

[†]*Computation Research Division, Lawrence Berkeley National Laboratory, Berkeley, CA*

[‡]*Department of Chemistry, University of Washington, Seattle, WA*

E-mail: rvanbeeumen@lbl.gov; dbwy@uw.edu; jkasper2@uw.edu; cyang@lbl.gov; egng@lbl.gov;
xqli@uw.edu



Abstract

The *ab initio* description of the spectral interior of the absorption spectrum poses both a theoretical and computational challenge for modern electronic structure theory. Due to the often spectrally dense character of this domain in the quantum propagator's eigenspectrum for medium-to-large sized systems, traditional approaches based on the partial diagonalization of the propagator often encounter oscillatory and stagnating convergence. Alternatively, electronic structure methods which solve the molecular

response problem through the solution of spectrally shifted linear systems, such as the complex polarization propagator, offer an alternative approach which is agnostic to the underlying spectral density or domain location. This generality comes at a seemingly high computational cost associated with solving a large linear system for each spectral shift in some discretization of the spectral domain of interest. In this work, we present a novel, adaptive solution to this high computational overhead based on model order reduction techniques via interpolation. Model order reduction reduces the computational complexity of mathematical models and is ubiquitous in the simulation of dynamical systems and control theory. The efficiency and effectiveness of the proposed algorithm in the *ab initio* prediction of X-Ray absorption spectra is demonstrated using a test set of challenging water clusters which are spectrally dense in the neighborhood of the oxygen *K*-edge. Based on a single, user defined tolerance we automatically determine the order of the reduced models and approximate the absorption spectrum up to the given tolerance. We also illustrate that this automatically determined order only slightly increases with the problem dimension, compared to a linear increase of the number of eigenvalues inside the energy window. Furthermore, we observed that the computational cost of the proposed algorithm only scales quadratically with respect to the problem dimension.

1 Introduction

With recent advances in laser light source technology, X-ray absorption spectroscopy (XAS) has become an important probative tool in chemical physics.¹ The ability of XAS to simultaneously characterize both the electronic and geometrical structure of chemical systems has made it indispensable in the fields of catalysis and photophysics.²⁻⁶ However, despite the capability of XAS to obtain a wealth of chemically relevant information, the complexity of experimentally obtained XAS spectra often requires a theoretical supplement to obtain a meaningful interpretation of the query phenomenon.^{7,8} Thus, the ability to properly describe

the high-energy electronic excitations of molecular systems theoretically is critical in modern electronic structure theory.

In light of its importance in physical chemistry, the prediction of XAS properties poses an interesting challenge for traditional electronic structure methods. This challenge is rooted in the fact that the X-Ray region is buried deep within the eigenspectrum of the Hamiltonian and is often spectrally dense. For example, in near edge X-Ray absorption fine structure (NEXAFS) spectroscopy, the spectrum consists of many excited states that correspond to excitations of core electrons to diffuse quasi bound levels. Thus, as system size increases, the number of states in the given energy region increases dramatically. Further, it is important to note that, because very large basis sets are often required to properly describe the rather diffuse nature of these excited states, the increase in complexity leads to poor scaling with system size.

Many electronic structure methods have been extended to the description of high-energy, X-ray electronic excitations in recent years. In the time domain, real-time density functional theory⁹⁻¹¹ has been shown to excellently reproduce the X-ray *K*-edge for molecules within relatively short simulation times.^{12,13} For large systems, however, time-domain methods have difficulty taking full advantage of concurrency on modern computing architectures, and are thus not yet a sustainable avenue in routine theoretical inquiry of these phenomena. In contrast, frequency domain approaches are often favored in these types of calculations as they may be cast as computationally scalable linear algebra problems which are well suited for today's computers. Frequency domain approaches to treat electronic excitations may be separated into two, equivalent categories: methods which aim to obtain a spectral decomposition of the quantum propagator, i.e. eigenproblem based methods, and methods which solve the response problem directly through the solution of linear systems of equations.

Recasting electronic structure methods into eigenproblems has long been an attractive frequency domain method for excited states. Through knowledge of the poles (eigenroots) of the quantum propagator, one has direct access to information regarding the electronic

excitations (resonances) of the molecular system. In addition, such a spectral decomposition may be used to treat off-resonant perturbations through interpolation schemes known as sum-over-states expressions. Much work has gone into the development of these methods in both wave function theory, such as those based on the coupled-cluster (CC)^{14–18} and algebraic diagrammatic construction (ADC)^{19,20} expansions of the many-body wave function, and density functional theory, such as the linear response time-dependent density functional theory (TD-DFT).^{21,22} These methods have been shown to accurately predict and reproduce both low-^{23,24} and high-energy^{12,25–30} electronic excitations in molecular systems. Despite their accuracy, however, eigenproblem based methods possess an inherent challenge in the description of high-energy excited states when the eigenroots of interest are buried deep in the eigenspectrum. Traditional methods used to partially diagonalize the propagator, such as the block-Davidson method,^{31–33} are designed to converge to the extreme ends of the eigenspectrum with no built-in mechanism to establish the spectrum’s interior. Several approaches have been described to overcome this problem,³⁴ including energy specific^{25,27} and restricted energy window methods^{28–30} when the eigenroots of interest are well-separated. Further, in spectrally dense regions of the propagator’s eigenspectrum, iterative diagonalization algorithms require the resolution of many more roots than is often practical to ensure smooth convergence.

Methods which solve the response problem through the solutions of linear systems offer an attractive alternative to eigenproblem based approaches in the description of high-energy excitations because they have an intrinsic mechanism to probe the interior of the energy spectrum. In these methods, the probing frequency of the applied perturbation is a chosen parameter.^{35,36} Thus, the interior of the spectrum is easily probed through a number of solutions of linear system of equations in the desired frequency domain. This simplicity does, however, come at a seemly significant computational cost compared to eigenproblem based methods. While eigenproblems are able to directly obtain many poles of the eigenspectrum simultaneously, one must solve the linear problem many times over some discretization of the

frequency domain to obtain similar results. In general, this discretization must be quite dense to achieve a reasonable accuracy and thus can be more expensive than their eigenproblem based counterparts. Approaches using linear systems and based on the complex polarization propagator (CPP), such as CPP-CC³⁷⁻³⁹ and TD-DFT,⁴⁰ have been shown to be successful in the description of both high and low energy properties of molecular systems and have been extended to relativistic Hamiltonians as well.⁴⁰⁻⁴⁶

In this work, we introduce a general framework for the prediction of spectrally interior molecular response properties based on model order reduction (MOR) via interpolation. Model order reduction techniques have been successfully applied in different fields of computation science and engineering, where it reduces the computational complexity of mathematical models in numerical simulations. Example, among others, are structural dynamics, sound and vibration analysis, and control theory.⁴⁷ The MOR algorithm proposed in this paper aims to overcome the large computational overhead associated with the spectral discretization required by linear system based methods while maintaining the accuracy associated with eigenproblem based methods. Further, the proposed algorithm will be shown to allow for the massively scalable parallelism that is well suited for modern computing architectures.

2 Linear response and absorption spectrum

In the semi-classical theory of molecular light-matter interaction within the electric dipole approximation, the isotropic absorption cross section for the interaction with plane-polarized light, $\sigma(\omega)$, at a particular perturbing frequency, ω , is proportional to the trace of the dynamic polarizability tensor, $\boldsymbol{\alpha}(\omega)$,

$$\sigma(\omega) \propto \text{Im} (\text{Tr} [\boldsymbol{\alpha}(\tilde{\omega})]), \quad \tilde{\omega} = \omega + i\eta, \quad (1)$$

where $\eta > 0$ is a small damping parameter to ensure the convergence of $\boldsymbol{\alpha}$ in the spectral neighborhoods of resonant perturbations. Within the linear response regime of the first-order

polarization propagator approximation (FOPPA),⁴⁸ the dynamic polarizability tensor may be written as

$$\boldsymbol{\alpha}(\tilde{\omega}) = \mathbf{d}^\top \mathbf{G}^{-1}(\tilde{\omega}) \mathbf{d}, \quad \mathbf{d} = \begin{bmatrix} \mathbf{d}_x & \mathbf{d}_y & \mathbf{d}_z \\ \mathbf{d}_x & \mathbf{d}_y & \mathbf{d}_z \end{bmatrix}. \quad (2)$$

Here, $\{\mathbf{d}_i \mid i \in \{x, y, z\}\}$ is the set of dipole operators expressed in the molecular orbital (MO) basis, and $\mathbf{G}(\tilde{\omega})$ is the first-order polarization propagator. In the following algorithm developments, we restrict the discussion to the FOPPA using a Hartree–Fock reference (TD-HF), although the algorithm presented is completely general to any choice of propagator or reference. Within TD-HF, $\mathbf{G}(\tilde{\omega})$ may be written as

$$\mathbf{G}(\tilde{\omega}) = \mathbf{H} - \tilde{\omega} \mathbf{S}, \quad (3)$$

where

$$\mathbf{H} = \begin{bmatrix} \mathbf{A} & \mathbf{B} \\ \mathbf{B} & \mathbf{A} \end{bmatrix}, \quad \mathbf{S} = \begin{bmatrix} \mathbf{I} & \mathbf{0} \\ \mathbf{0} & -\mathbf{I} \end{bmatrix}, \quad (4)$$

with $\mathbf{S} = \mathbf{S}^\top = \mathbf{S}^{-1}$ and

$$A_{ai,bj} = \delta_{ij} \delta_{ab} (\epsilon_a - \epsilon_i) + (ai||bj), \quad (5)$$

$$B_{ai,bj} = (ab||ij). \quad (6)$$

Here, we have adopted the convention of denoting occupied MOs with indices i, j, k, \dots and virtual (unoccupied) MOs with indices a, b, c, \dots . $\{\epsilon_p\}$ is taken to be the set of canonical Hartree–Fock MO eigenenergies and the moieties $(\cdot||\cdot)$ are the MO basis representation of the anti-symmetried electron-repulsion integrals in Mulliken notation. In this work, we restrict our treatment to the use of strictly real MOs to allow for further simplification of the working expressions.

In order to study the spectrum of the pencil (\mathbf{H}, \mathbf{S}) let

$$\mathbf{\Omega} = \mathbf{S}^{-1}\mathbf{H} = \begin{bmatrix} \mathbf{A} & \mathbf{B} \\ -\mathbf{B} & -\mathbf{A} \end{bmatrix}. \quad (7)$$

Although the matrix $\mathbf{\Omega}$ is non-symmetric, it has a number of special properties.^{14,49,50} If \mathbf{H} is positive definite, it may be shown that $\mathbf{\Omega}$ possesses a structured eigendecomposition,⁵¹ i.e.,

$$\begin{bmatrix} \mathbf{A} & \mathbf{B} \\ -\mathbf{B} & -\mathbf{A} \end{bmatrix} = \begin{bmatrix} \mathbf{U} & \mathbf{V} \\ \mathbf{V} & \mathbf{U} \end{bmatrix} \begin{bmatrix} \mathbf{\Lambda} & \mathbf{0} \\ \mathbf{0} & -\mathbf{\Lambda} \end{bmatrix} \begin{bmatrix} \mathbf{U} & -\mathbf{V} \\ -\mathbf{V} & \mathbf{U} \end{bmatrix}^{\top} \quad (8)$$

where $\mathbf{\Lambda} = \text{diag}(\lambda_1, \dots, \lambda_n)$ consists of strictly positive eigenvalues, and the eigenvectors are normalized with respect to the metric \mathbf{S} ,

$$\begin{bmatrix} \mathbf{U} & -\mathbf{V} \\ -\mathbf{V} & \mathbf{U} \end{bmatrix}^{\top} \begin{bmatrix} \mathbf{U} & \mathbf{V} \\ \mathbf{V} & \mathbf{U} \end{bmatrix} = \mathbf{I}. \quad (9)$$

As \mathbf{H} is taken to be real in this work, it possesses additional properties that may be exploited in the development of efficient algorithms for estimating the absorption spectrum of the target system. In particular, we may apply the following similarity transformation

$$\mathbf{T} = \frac{1}{\sqrt{2}} \begin{bmatrix} \mathbf{I} & \mathbf{I} \\ -\mathbf{I} & \mathbf{I} \end{bmatrix}, \quad \mathbf{T}^{-1} = \mathbf{T}^{\top}, \quad (10)$$

to $\mathbf{G}(\tilde{\omega})$, yielding

$$\mathbf{T}^{\top}\mathbf{G}(\tilde{\omega})\mathbf{T} = \begin{bmatrix} \mathbf{K} & \mathbf{0} \\ \mathbf{0} & \mathbf{M} \end{bmatrix} - \tilde{\omega} \begin{bmatrix} \mathbf{0} & \mathbf{I} \\ \mathbf{I} & \mathbf{0} \end{bmatrix}, \quad (11)$$

where

$$\mathbf{M} \equiv \mathbf{A} + \mathbf{B}, \quad (12)$$

$$\mathbf{K} \equiv \mathbf{A} - \mathbf{B}, \quad (13)$$

which are, in most cases, positive definite. In this case, the polarizability tensor may be reformulated as

$$\boldsymbol{\alpha}(\tilde{\omega}) = \tilde{\mathbf{d}}^\top \tilde{\mathbf{G}}^{-1}(\tilde{\omega}) \tilde{\mathbf{d}}, \quad \tilde{\mathbf{d}} = \begin{bmatrix} \mathbf{d}_x & \mathbf{d}_y & \mathbf{d}_z \end{bmatrix}, \quad (14)$$

where

$$\tilde{\mathbf{G}}(\tilde{\omega}) = \mathbf{MK} - \tilde{\omega}^2 \mathbf{I}. \quad (15)$$

Note that the dimension of $\tilde{\mathbf{G}}(\tilde{\omega})$ is only half the dimension of $\mathbf{G}(\tilde{\omega})$. Furthermore, it can be shown that

$$\mathbf{M} = (\mathbf{X} - \mathbf{Y})\boldsymbol{\Lambda}(\mathbf{X} - \mathbf{Y})^\top, \quad (16)$$

$$\mathbf{K} = (\mathbf{X} + \mathbf{Y})\boldsymbol{\Lambda}(\mathbf{X} + \mathbf{Y})^\top, \quad (17)$$

and

$$(\mathbf{X} - \mathbf{Y})^\top (\mathbf{X} + \mathbf{Y}) = \mathbf{I}, \quad (18)$$

such that the eigenvalues $\pm\boldsymbol{\Lambda}$ may be computed by

$$\mathbf{MK} = (\mathbf{X} - \mathbf{Y})\boldsymbol{\Lambda}^2(\mathbf{X} + \mathbf{Y})^\top. \quad (19)$$

Remark that by making use of \mathbf{MK} , the dimension of the eigenvalue problem is also reduced by a factor of 2.⁵²

3 Estimating absorption spectrum without explicitly computing eigenvalues and eigenvectors

The most straightforward way to evaluate the absorption spectrum is to compute eigenvalues and the corresponding eigenvectors of (\mathbf{H}, \mathbf{S}) . However, as we indicated earlier, when the dimension of \mathbf{H} and \mathbf{S} becomes large, this approach can be prohibitively expensive.

It has been shown in⁵³ that a special \mathbf{K} -inner product Lanczos algorithm can be used to provide a good approximation to the overall structure of the absorption spectrum without explicitly computing the eigenvalues and eigenvectors of (\mathbf{H}, \mathbf{S}) . In particular, the Lanczos algorithm can reveal major absorption peaks in the low frequency region of the spectrum without too many iterations. However, the algorithm gives limited resolution of the absorption spectrum in the middle of the spectrum because the Krylov subspace constructed by the Lanczos iteration contains little spectral information associated with interior eigenvalues of (\mathbf{H}, \mathbf{S}) .

We now propose an alternative way to evaluate the absorption spectrum without explicitly computing the eigenvalues and eigenvectors of (\mathbf{H}, \mathbf{S}) . This scheme focuses on approximating the dynamic polarizability tensor $\boldsymbol{\alpha}(\tilde{\omega})$ defined in (2) and the absorption spectrum $\sigma(\omega)$ defined in (1) within a specific energy window directly.

Firstly, observe that the dynamic polarizability tensor (2) may be viewed simply as the expectation value of the inverse of $\mathbf{H} - \tilde{\omega}\mathbf{S}$. Hence, the evaluation of $\boldsymbol{\alpha}(\tilde{\omega})$ may be recast into a problem of solving linear equations, i.e., for a specific frequency ω , we can directly evaluate the absorption spectrum (1) as follows

$$\sigma(\omega) \propto \text{Im} \left(\text{Tr} \left[\mathbf{d}^\top \mathbf{x}(\tilde{\omega}) \right] \right), \quad (20)$$

where \mathbf{x} is the solution of the linear system

$$(\mathbf{H} - \tilde{\omega}\mathbf{S}) \mathbf{x}(\tilde{\omega}) = \mathbf{d}. \quad (21)$$

Secondly, the dynamic polarizability tensor (2) may also be viewed as the transfer function, i.e., the relation between input and output, of the linear dynamical system (see appendix A.1)

$$\begin{cases} (\mathbf{H} - \tilde{\omega}\mathbf{S}) \mathbf{x}(\tilde{\omega}) = \mathbf{d} \\ \mathbf{y}(\omega) = \mathbf{d}^\top \mathbf{x}(\tilde{\omega}) \end{cases}. \quad (22)$$

Consequently, the absorption spectrum can directly be obtained from the output variable \mathbf{y}

$$\sigma(\omega) \propto \text{Im} (\text{Tr} [\mathbf{y}(\omega)]). \quad (23)$$

In order to evaluate the output \mathbf{y} of system (22) for a given frequency, we again need to solve a linear system of the form (21).

Finally, by exploiting the block structure of \mathbf{H} and performing a state space transformation with (10) (see appendix A.2), we obtain an equivalent linear dynamical system for (22), but with a halved order,

$$\begin{cases} (\mathbf{MK} - \tilde{\omega}^2\mathbf{I}) \tilde{\mathbf{x}}(\tilde{\omega}) = \tilde{\mathbf{d}} \\ \mathbf{y}(\omega) = 2\tilde{\mathbf{d}}^\top \mathbf{K} \tilde{\mathbf{x}}(\tilde{\omega}) \end{cases}, \quad (24)$$

such that we obtain the following, compact expressions for the dynamic polarizability tensor

$$\boldsymbol{\alpha}(\tilde{\omega}) = 2\tilde{\mathbf{d}}^\top \mathbf{K} (\mathbf{MK} - \tilde{\omega}^2\mathbf{I})^{-1} \tilde{\mathbf{d}}, \quad (25)$$

and the absorption spectrum

$$\sigma(\omega) \propto \text{Im} \left(\text{Tr} \left[\tilde{\mathbf{d}}^\top \mathbf{K} (\mathbf{MK} - \tilde{\omega}^2\mathbf{I})^{-1} \tilde{\mathbf{d}} \right] \right). \quad (26)$$

Note that the dimension of the linear systems to be solved in (26) is only half of the dimension of the linear system shown in (21).

Clearly, we cannot afford to evaluate $\sigma(\omega)$ for all ω 's. However, this connection to lin-

ear dynamical systems allows us to employ model order reduction (MOR) techniques (see appendix A.3) to reduce the number of full $\sigma(\omega)$ evaluations. More precisely, we construct a function $\hat{\sigma}(\omega)$ that approximates $\sigma(\omega)$ within a specific energy window $[\omega_{\min}, \omega_{\max}]$, but is much cheaper to evaluate. The construction of such an approximate function only requires solving a few linear systems of the form (21) or (24) at a few selected frequencies τ_j , $j = 1, 2, \dots, k$. The solutions of these linear systems are then used to construct a reduced order model which interpolates the full dynamic polarizability at τ_j , and provides an approximation to the dynamic polarizability tensor (2) at other frequencies within the predefined energy window. When k is small, both the construction and the evaluation of the reduced order model is significantly lower than other approaches that are either based on solving an eigenvalue problem or (21) at many different frequencies.

4 Model order reduction via interpolation

The absorption spectrum $\sigma(\omega)$ is clearly determined by the Hamiltonian which models the linear response of charge density to external perturbation. When the dimension of \mathbf{H} becomes large due to increase in molecule size (i.e., the number of atoms) or the size of the basis set, even the evaluation of (1) through solving linear equations can be costly. The main idea of model order reduction is to replace system (22) by a similar system with a lower dimensional $\hat{\mathbf{H}}$ that retains the main spectral features of \mathbf{H} within the energy window of interest. This technique is widely used for approximating the transfer function of a linear dynamical system (see appendix A).

Let us assume that the dimension of the matrix \mathbf{H} defined in (4) is $2n \times 2n$. The dimension of the lower dimensional matrix $\hat{\mathbf{H}}$ that we construct for the reduced order model is $3k \times 3k$, where $k \ll n$. One way to construct such a matrix is to first construct a subspace spanned by orthonormal columns of a matrix $\mathbf{V} \in \mathbb{R}^{2n \times 3k}$ and then project \mathbf{H} onto such a subspace

\mathbf{V} , i.e.,

$$\widehat{\mathbf{H}} = \mathbf{V}^\top \mathbf{H} \mathbf{V}. \quad (27)$$

If we also let $\widehat{\mathbf{S}} = \mathbf{V}^\top \mathbf{S} \mathbf{V}$ and $\widehat{\mathbf{d}} = \mathbf{V}^\top \mathbf{d}$, then the absorption spectrum can be approximated by

$$\widehat{\sigma}(\omega) \propto \text{Im} \left(\text{Tr} \left[\widehat{\mathbf{d}}^\top \left(\widehat{\mathbf{H}} - \omega \widehat{\mathbf{S}} \right)^{-1} \widehat{\mathbf{d}} \right] \right). \quad (28)$$

Clearly, the choice of the subspace \mathbf{V} is crucial in maintaining the fidelity of the reduced order model. The subspace we use to construct the reduced order model takes the form

$$\mathbf{V} = \text{span} \left[(\mathbf{H} - \tau_1 \mathbf{S})^{-1} \mathbf{d} \quad (\mathbf{H} - \tau_2 \mathbf{S})^{-1} \mathbf{d} \quad \cdots \quad (\mathbf{H} - \tau_k \mathbf{S})^{-1} \mathbf{d} \right], \quad (29)$$

where τ_j , $j = 1, 2, \dots, k$ are the interpolation frequencies carefully chosen within the energy window of interest to ensure that

$$\sigma(\omega) \approx \widehat{\sigma}(\omega), \quad (30)$$

for all ω in the energy window of interest. It follows from the way \mathbf{V} is constructed in (29) that $\widehat{\boldsymbol{\alpha}}$ interpolates $\boldsymbol{\alpha}$ at the interpolation frequencies, i.e.,

$$\boldsymbol{\alpha}(\tau_j) = \widehat{\boldsymbol{\alpha}}(\tau_j), \quad j = 1, 2, \dots, k. \quad (31)$$

Algorithm 1 summarizes the construction of the reduced order model and how it is used to obtain an approximation of the absorption spectrum within an energy window of interest. Clearly, the higher the model order k , the more accurate the approximation is. In the next section, we will show that even for a relatively small k , we can obtain a quite accurate approximation to $\sigma(\omega)$ in an interior spectral window that contains thousands of eigenvalues.

Although algorithm 1 provides a general framework for constructing a reduced order model for estimating the absorption spectrum defined by (\mathbf{H}, \mathbf{S}) , it is more efficient to exploit the structure of (\mathbf{H}, \mathbf{S}) and construct a reduced order model for (24) instead. Such a reduced

Algorithm 1: Absorption spectrum via model order reduction

Input : Matrices $\mathbf{H}, \mathbf{S}, \mathbf{d}$,
 Interpolation frequencies $\tau_1, \tau_2, \dots, \tau_k$,
 Frequencies $\omega_1, \omega_2, \dots, \omega_N$, and η .

Output: Absorption spectrum $\hat{\sigma}(\omega_1), \hat{\sigma}(\omega_2), \dots, \hat{\sigma}(\omega_N)$.

for $j = 1, 2, \dots, k$ **do**

- 1 | Linear system solve $\mathbf{x}_j = (\mathbf{H} - \tau_j \mathbf{S})^{-1} \mathbf{d}$.
- end**
- 2 QR factorization $\mathbf{X} = \mathbf{V}\mathbf{R}$.
- 3 Construct $\hat{\mathbf{H}} = \mathbf{V}^\top \mathbf{H}\mathbf{V}$, $\hat{\mathbf{S}} = \mathbf{V}^\top \mathbf{S}\mathbf{V}$, and $\hat{\mathbf{d}} = \mathbf{V}^\top \mathbf{d}$.
- for** $j = 1, 2, \dots, N$ **do**
- 4 | Compute $\hat{\sigma}(\omega_j) = \text{Im} \left(\text{Tr} \left[\hat{\mathbf{d}}^\top \left(\hat{\mathbf{H}} - (\omega_j + i\eta) \hat{\mathbf{S}} \right)^{-1} \hat{\mathbf{d}} \right] \right)$.
- end**

order model can be obtained by projecting (24) onto a subspace defined by

$$\tilde{\mathbf{V}} = \text{span} \left[(\mathbf{M}\mathbf{K} - \tau_1^2 \mathbf{I})^{-1} \tilde{\mathbf{d}} \quad (\mathbf{M}\mathbf{K} - \tau_2^2 \mathbf{I})^{-1} \tilde{\mathbf{d}} \quad \dots \quad (\mathbf{M}\mathbf{K} - \tau_k^2 \mathbf{I})^{-1} \tilde{\mathbf{d}} \right], \quad (32)$$

where $\tau_j, j = 1, 2, \dots, k$ are again the interpolation frequencies. Because the matrix $\mathbf{M}\mathbf{K}$ is self-adjoint with respect to the \mathbf{K} -inner product, it is more convenient to carry out the projection using the \mathbf{K} -inner product and projecting $\mathbf{M}\mathbf{K}$ onto a subspace spanned by a \mathbf{K} -orthonormal basis, i.e., we should \mathbf{K} -orthonormalize columns of (32) so that $\tilde{\mathbf{V}}^\top \mathbf{K} \tilde{\mathbf{V}} = \mathbf{I}$ is satisfied. If we let

$$\widehat{\mathbf{M}\mathbf{K}} = \tilde{\mathbf{V}}^\top \mathbf{K} \mathbf{M} \mathbf{K} \tilde{\mathbf{V}}, \quad (33)$$

$$\hat{\mathbf{d}} = \tilde{\mathbf{V}}^\top \mathbf{K} \tilde{\mathbf{d}}, \quad (34)$$

then the approximation to the absorption spectrum provided by the structure exploiting

reduced order model can be expressed by

$$\hat{\sigma}(\omega) \propto \text{Im} \left(\text{Tr} \left[\hat{\mathbf{d}}^\top \left(\widehat{\mathbf{MK}} - \tilde{\omega}^2 \mathbf{I} \right)^{-1} \hat{\mathbf{d}} \right] \right). \quad (35)$$

By making use of the block structure of \mathbf{H} , we can prove that (28) and (35) are equivalent. However, the latter is cheaper to construct, both in terms of the number of floating point operations and memory usage, since it only involves matrices of size $n \times n$ and vectors of size n . The structure exploiting model order reduction algorithm for approximating the absorption spectrum is outlined in algorithm 2.

Note that both algorithms 1 and 2 require a choice of the interpolation frequencies τ_j . The number of these interpolation frequencies and their locations solely determine the quality of the absorption spectrum approximations. The simplest way to choose these interpolation frequencies is to partition the energy window of interest evenly by a uniform interpolation grid. However, because the absorption spectrum can be highly oscillatory in certain regions within the energy window, a very fine grid may be needed to resolve the high oscillation. As a result, the order of the reduced order model, which is proportional to the number of

Algorithm 2: Absorption spectrum via structure exploiting model order reduction

Input : Matrices $\mathbf{M}, \mathbf{K}, \tilde{\mathbf{d}}$,
Interpolation frequencies $\tau_1, \tau_2, \dots, \tau_k$,
Frequencies $\omega_1, \omega_2, \dots, \omega_N$, and η .

Output: Absorption spectrum $\hat{\sigma}(\omega_1), \hat{\sigma}(\omega_2), \dots, \hat{\sigma}(\omega_N)$.

for $j = 1, 2, \dots, k$ **do**

1 | Linear system solve $\tilde{\mathbf{x}}_j = (\mathbf{MK} - \tau_j^2 \mathbf{I})^{-1} \tilde{\mathbf{d}}$.

end

2 QR factorization $\tilde{\mathbf{X}} = \tilde{\mathbf{V}}\tilde{\mathbf{R}}$, with $\tilde{\mathbf{V}}^\top \mathbf{K}\tilde{\mathbf{V}} = \mathbf{I}$.

3 Construct $\widehat{\mathbf{MK}} = \tilde{\mathbf{V}}^\top \mathbf{K}\mathbf{M}\tilde{\mathbf{V}}$ and $\hat{\mathbf{d}} = \tilde{\mathbf{V}}^\top \mathbf{K}\tilde{\mathbf{d}}$.

for $j = 1, 2, \dots, N$ **do**

4 | Compute $\hat{\sigma}(\omega_j) = \text{Im} \left(\text{Tr} \left[\hat{\mathbf{d}}^\top \left(\widehat{\mathbf{MK}} - (\omega_j + i\eta)^2 \mathbf{I} \right)^{-1} \hat{\mathbf{d}} \right] \right)$.

end

interpolation frequencies, can be exceedingly high.

A more effective strategy for choosing the interpolation frequencies is to choose these frequencies in an adaptive fashion. We now propose a refinement strategy, which is graphically illustrated in fig. 1. To start this procedure, we choose in the first level a coarse, uniform grid of interpolation frequencies (marked by \blacksquare) to construct the level-1 reduced order model. The set of interpolation frequencies is refined by adding the midpoints (marked by \blacktriangle) between two adjacent level-1 interpolation frequencies. This enlarged set forms the second level of interpolation frequencies, yielding a more accurate level-2 reduced order model. Next, we choose the midpoints between two adjacent level-2 interpolation frequencies as candidates (marked by \circ) to enlarge the set in the third level. We also estimate the approximation error by computing the relative difference between the level-1 and level-2 reduced order models for the entire energy window. If the error estimate at an interval between two adjacent level-2 interpolation frequencies is above a prescribed error tolerance, the midpoint (marked by \bullet) is added to the existing set of interpolation frequencies. The enlarged set results in an even more accurate level-3 reduced order model. This refinement process continues until the error estimate at the entire energy window is below the threshold or when the refined model order exceeds an prescribed upper bound.

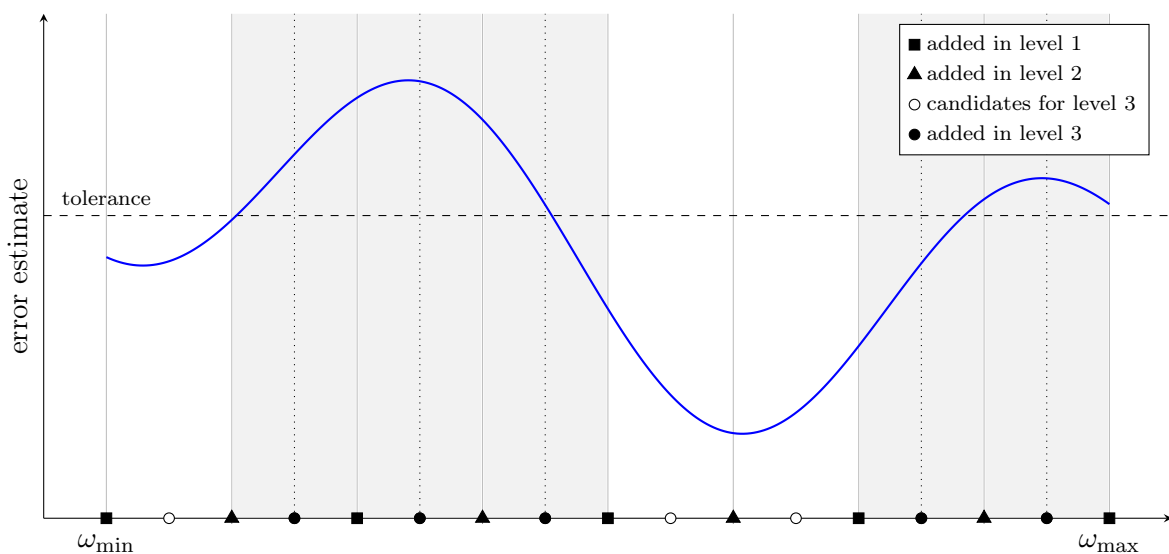


Figure 1: Adaptive refinement strategy for selecting the interpolation frequencies.

5 Computational results

The proposed automatic MOR algorithm has been implemented in the Chronus Quantum software package⁵⁴ and in MATLAB[§]. The following numerical experiments were performed on a Cray XC40 using a single Haswell Intel Xeon compute node (E5-2698 v3 @2.3 GHz, 2x16 cores, 128 GB DDR4 RAM). All of the water cluster test cases were performed using the 6-31G basis set without the use of molecular symmetry and were chosen for their dense spectral character in the X-Ray spectral domain.

The implementation of the MOR utilizes a synchronized approach to the Generalized Minimum Residual (GMRES)⁵⁵ algorithm for the solution of the linear systems. In this approach,⁵⁶ each linear system is solved individually via the standard GMRES algorithm but its matrix-vector products (GEMVs), which are the dominant cost, are synchronized and preformed in batches. Hence, the GEMVs become matrix-matrix products (GEMMs) and allow for optimal efficiency and cache utilization through the use of Level 3 BLAS operations. In all experiments we used a block size of 12, coming from combining the 3 dipole vectors of 4 interpolation frequencies.

Several numerical experiments were performed to demonstrate the performance and accuracy of the proposed MOR algorithms. Since the interpolation points are merely used to construct a reduced order model, it is conceivable that we may choose them to be real numbers instead of complex numbers that contain a small imaginary damping factor. The advantage of choosing real interpolation points is that all linear systems can be solved in real arithmetic. However, as we will see below, this approach may not lead to any performance gain.

We also examined how the order of the reduced order model changes as the size of the molecular system increases as well as the overall computational scaling of the proposed method using the aforementioned water clusters. Numerical comparisons are made to the Lorentzian broadened poles of the propagator using the oscillator strengths.⁵⁷⁻⁵⁹

[§]<https://bitbucket.org/roelvb/mor4absspectrum>

5.1 Real versus complex interpolation frequencies

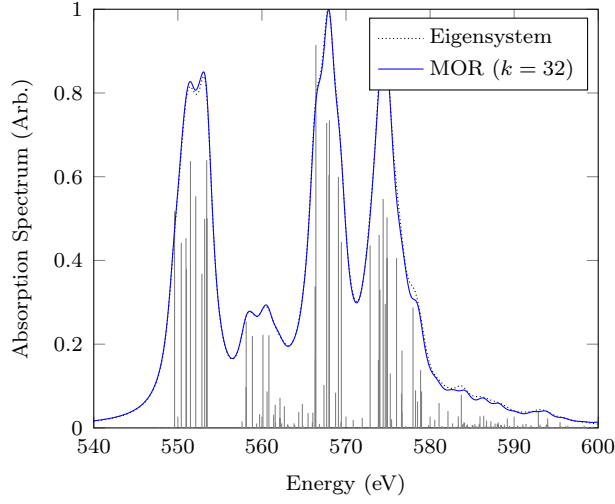
We start with a cluster of 5 water molecules and are interested in computing the absorption spectrum in the energy window [540 eV, 600 eV]. The dimension of the matrix \mathbf{H} (4) was $2n = 4,000$ and \mathbf{H} had 356 eigenvalues in the energy window. The damping factor was $\eta = 1$ eV and the tolerance for solving the linear systems was set to 10^{-6} .

In the first experiment, we used a fixed order $k = 32$ for the reduced order models and only varied the interpolation frequencies τ_j , $j = 1, 2, \dots, k$. We computed the absorption spectrum by algorithms 1 and 2 for both real $\tau_j = \omega_j$ and complex $\tau_j = \omega_j + i\eta$, where ω_j were uniformly selected in the energy window. The corresponding results are presented in fig. 2 and in the top part of table 1. Note that by using complex interpolation frequencies τ_j , we obtained good approximations to the absorption spectrum from both algorithms 1 and 2. On the other hand, the use of real τ_j resulted in much less accurate approximations. This can be explained by noticing that some of the (real) interpolation frequencies are very close to the (real) eigenvalues of (\mathbf{H}, \mathbf{S}) or \mathbf{MK} , resulting in ill-conditioned linear systems to be solved. However, this can be avoided when complex interpolation frequencies are used.

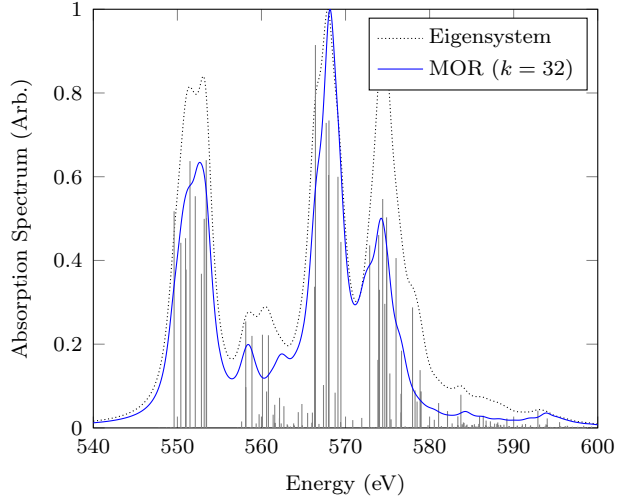
Next, we repeated the previous experiment but chose the interpolation frequencies via the adaptive refinement strategy introduced in section 4. As error estimate we used the difference of the normalized absorption spectrum between two consecutive levels. The tolerance was set to 0.01, which corresponded to a 1 percent change in the overall absorption spectrum

Table 1: Cluster of 5 H₂O molecules: Real versus complex interpolation frequencies τ_j .

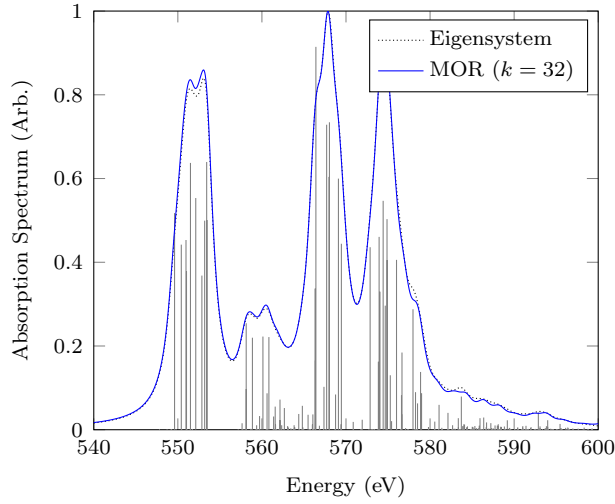
Algorithm	k	GEMMs	Wall (s)
Algorithm 1: complex τ_j	32	710	20.8
Algorithm 1: real τ_j	32	943	10.5
Algorithm 2: complex τ_j	32	585	9.9
Algorithm 2: real τ_j	32	869	5.5
Algorithm 1: complex τ_j	71	1,868	54.9
Algorithm 1: real τ_j	198	6,287	77.0
Algorithm 2: complex τ_j	68	1,533	35.9
Algorithm 2: real τ_j	204	5,981	42.1



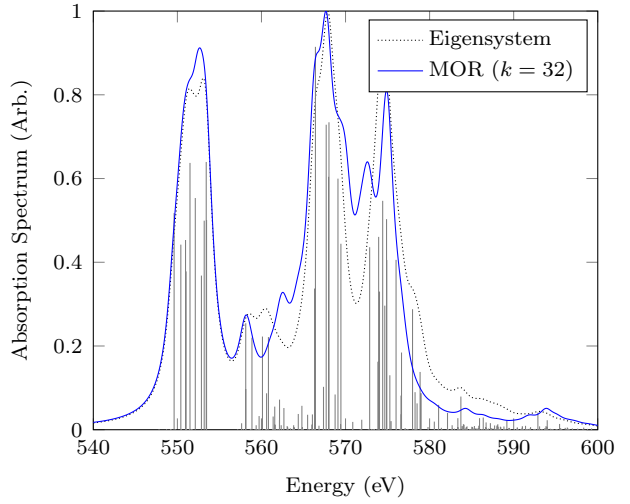
(a) Algorithm 1: complex τ_j



(b) Algorithm 1: real τ_j



(c) Algorithm 2: complex τ_j



(d) Algorithm 2: real τ_j

Figure 2: Cluster of 5 H_2O molecules: Real versus complex interpolation frequencies τ_j for fixed reduced order $k = 32$. Numerical comparisons to the Lorentzian broadened poles of the propagator, labelled Eigensystem.

on the window [540 eV, 600 eV]. This resulted in reduced order models of different orders k , reported in the bottom part of table 1. Firstly, we observe that in terms of the order k the use of complex interpolation frequencies has an significant advantages over real ones. Secondly, we also observe that the adaptive refinement strategy for algorithms 1 and 2 resulted in very similar orders k when the same type of interpolation frequencies are used.

The corresponding computational work for the previous two experiments is reported in table 1. At first, we observe that for both fixed as well as adaptive model orders k the computational cost and wall time for algorithm 2 was significantly lower than the ones for algorithm 1. This is expected because both methods are mathematically equivalent and the former only deals with linear systems of half the dimension of the latter. Furthermore, although real interpolation frequencies have the advantage that we only need to solve *real* linear systems, we observe that in case of adaptively chosen model orders k the use of complex interpolation frequencies was much cheaper.

5.2 Computational scaling

We now consider water clusters consisting of 5, 10, 15, 20, and 25 water molecules. The corresponding dimensions are shown in table 2. The energy window [540 eV, 600 eV] and damping factor $\eta = 1$ eV were the same as for the previous experiments. We computed the absorption spectrum via algorithm 2 with complex interpolation frequencies chosen in the adaptive way. The obtained absorption spectra are shown in fig. 4.

Table 2: Cluster of H₂O molecules: MOR results for the absorption spectra computed via algorithm 2 with adaptively chosen complex interpolation frequencies.

#	Waters		GMRES tol = 10 ⁻⁴			GMRES tol = 10 ⁻⁵			GMRES tol = 10 ⁻⁶		
	n	# λ	k	GEMMs	Wall (s)	k	GEMMs	Wall (s)	k	GEMMs	Wall (s)
5	2,000	356	66	868	19.0	68	1,268	27.4	68	1,533	35.9
10	8,000	1,376	102	1,791	168.7	91	2,483	285.2	90	3,226	416.5
15	18,000	3,032	92	2,053	844.0	87	3,105	1,290.8	87	4,129	1,711.7
20	32,000	5,282	120	2,651	3,210.0	97	3,359	4,161.9	97	4,583	5,818.5
25	50,000	8,172	121	2,857	7,559.5	101	3,736	9,389.1	101	5,123	13,690.2

The MOR results are given in table 2, where we present the orders k of the reduced order models, the total number of GEMMs, and the total wall time for different GMRES convergence tolerances. Firstly, we observe that the order k of the reduced order models only slightly increases with the number of waters, whereas the number of eigenvalues inside the energy window, $\#\lambda$, grows linearly with respect to the problem dimension. Secondly, the order k decreases for increasing GMRES convergence tolerances and seems to stagnate around 10^{-5} . Moreover, there were no visual differences any more between the obtained absorption spectra for GMRES tolerances 10^{-5} and 10^{-6} .

The total wall time and number of GEMMs are also shown in fig. 3. The left figure illustrates that the wall time scales quadratically with respect to the problem dimension, compared to a cubic scaling for a full diagonalization. Moreover, the right figure shows that the number of GEMMs only scales logarithmically, compared to an expected linear scaling for iterative eigensolvers since the number of eigenvalues inside the energy window grows linearly.

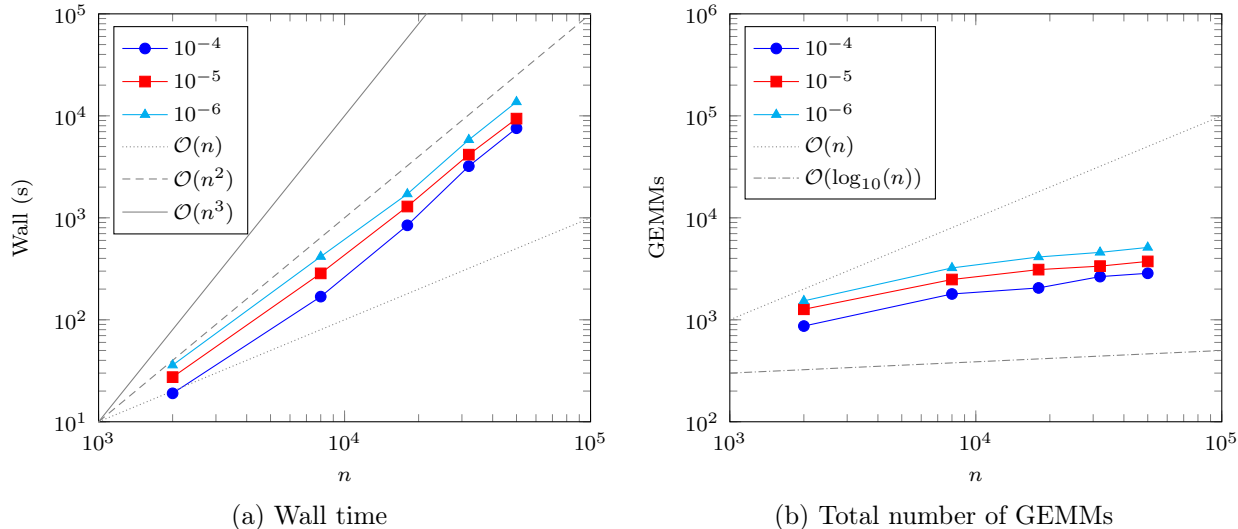


Figure 3: Cluster of H_2O molecules: MOR results for the absorption spectra computed via algorithm 2 with adaptively chosen complex interpolation frequencies. The comparisons are made for GMRES convergence tolerances of 10^{-4} , 10^{-5} , and 10^{-6} .

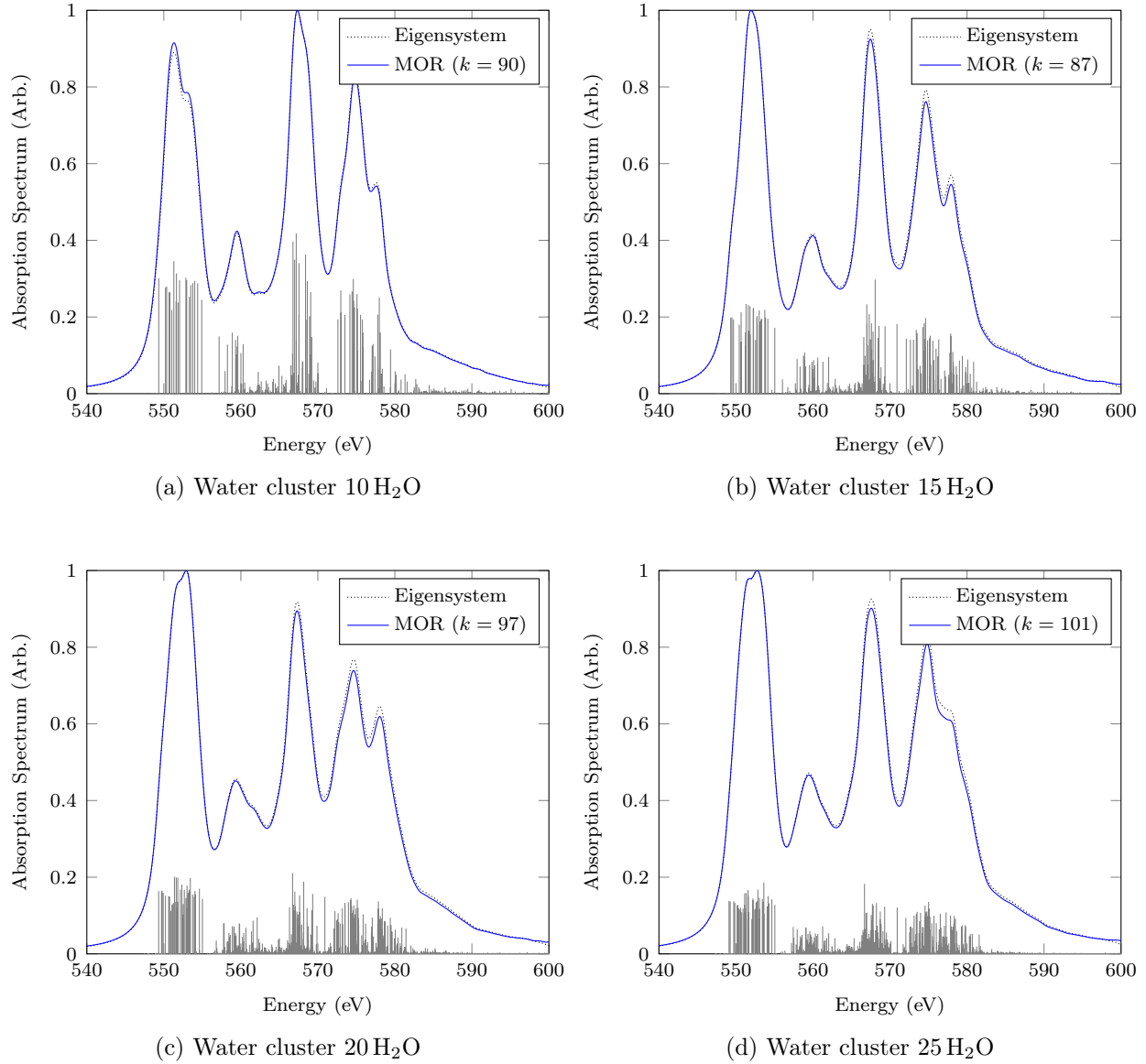


Figure 4: Cluster of H₂O molecules: Absorption spectra computed via algorithm 2 with adaptively chosen complex interpolation frequencies. Numerical comparisons to the Lorentzian broadened poles of the propagator, labelled Eigensystem.

6 Conclusion

In this work, we have presented a novel, adaptive algorithm for the *ab initio* prediction of the absorption spectrum based on model order reduction techniques applied to the quantum propagator. While this approach is general to any spectral domain, the power of the proposed method is in those spectral domains which are dense and interior in the propagator's eigenspectrum. The accuracy and efficiency of this method to predict the X-Ray absorption spectrum have been demonstrated using a series of water clusters. Water clusters were chosen as an especially challenging case study as the propagator is spectrally dense in the spectral neighborhood of the water's oxygen *K*-Edge. The numerical experiments have shown that complex interpolation frequencies should be preferred over real ones and that in this case the order of the reduced order models only slightly increases with the problem dimension, in contrast to the rapid growth of the number of eigenvalues inside the energy window. Moreover, the wall time for the proposed model order reduction algorithm scales only quadratically with respect to the dimension of the problem, compare to cubic scaling for eigenvalue based algorithms. While results were presented only for the TD-HF method, the proposed adaptive MOR algorithm is general to any choice reference, propagator, or perturbation. Further, although it is not expressly considered in this work, this technique is well suited for parallelism on a massive scale as each of the linear system solutions is completely independent from the other, thus allowing for minimal communication. With the proposed MOR algorithm, routine study of X-Ray absorption spectra for medium-to-large sized systems is feasible.

Acknowledgement

This work was partly supported by the Scientific Discovery through Advanced Computing (SciDAC) program (R. V. B., C. Y. and E. G. Ng) and the IDREAM Energy Frontier Research Center (D. B. W-Y, J. M. K. and X. L.), funded by U.S. Department of Energy,

Office of Science, Advanced Scientific Computing Research and Basic Energy Sciences. The development of the Chronus Quantum software is supported by the National Science Foundation (CHE-1565520 to X.L.). The authors thank the National Energy Research Scientific Computing (NERSC) center for making computational resources available to them. The authors are also grateful to Dr. Meiyue Shao for helpful discussions.

A Linear dynamical systems

In this appendix, we briefly review linear dynamical systems and point out its connection to the computation of the absorption spectrum within the first order polarization propagator approximation.

A.1 Linear dynamical systems

We consider the linear multiple-input multiple-output (MIMO) system

$$\Sigma = \begin{cases} (\mathbf{H} - s\mathbf{S}) \mathbf{x}(s) = \mathbf{b} u(s) \\ \mathbf{y}(s) = \mathbf{c}^\top \mathbf{x}(s) \end{cases}, \quad (36)$$

where s is the derivative or shift operator, $\mathbf{H} \in \mathbb{R}^{n \times n}$ and $\mathbf{S} \in \mathbb{R}^{n \times n}$ are the system matrices, $\mathbf{b} \in \mathbb{R}^{n \times m}$, and $\mathbf{c} \in \mathbb{R}^{n \times p}$. We call n the dimension (order) of the system Σ , $\mathbf{x} \in \mathbb{R}^{n \times m}$ the state vector, $u \in \mathbb{R}$ the input, and $\mathbf{y} \in \mathbb{R}^{p \times m}$ the output.⁴⁷ Note that the system Σ is completely characterized by the quadruple $(\mathbf{H}, \mathbf{S}, \mathbf{b}, \mathbf{c})$.

The transfer function of Σ is defined as

$$\gamma(s) = \mathbf{c}^\top (\mathbf{H} - s\mathbf{S})^{-1} \mathbf{b}, \quad (37)$$

and describes the relation between the input and output of Σ , i.e., $\mathbf{y}(s) = \gamma(s)u(s)$. For the remainder, we will assume that $u(s) \equiv 1$ for all s .

A.2 State space transformation

In some cases, it might be advantages to describe the system from a different point of view as the original one. Therefore, we can perform a state transformation \mathbf{T} , with $\det(\mathbf{T}) \neq 0$, yielding the transformed state

$$\tilde{\mathbf{x}} = \mathbf{T}^{-1}\mathbf{x}, \quad (38)$$

of the transformed system

$$\tilde{\Sigma} = \begin{cases} (\tilde{\mathbf{H}} - s\tilde{\mathbf{S}})\tilde{\mathbf{x}}(s) = \tilde{\mathbf{b}}u(s) \\ \mathbf{y}(s) = \tilde{\mathbf{c}}^\top\tilde{\mathbf{x}}(s) \end{cases}, \quad (39)$$

where $\tilde{\mathbf{H}} = \mathbf{T}^{-1}\mathbf{HT}$, $\tilde{\mathbf{S}} = \mathbf{T}^{-1}\mathbf{ST}$, $\tilde{\mathbf{b}} = \mathbf{T}^{-1}\mathbf{b}$, and $\tilde{\mathbf{c}}^\top = \mathbf{c}^\top\mathbf{T}$. Remark that Σ and $\tilde{\Sigma}$ have both the same transfer function as well as the same output. Therefore, we call the systems Σ and $\tilde{\Sigma}$ equivalent.

A.3 Reduced order models and moment matching

The evaluation of the transfer function of a system Σ requires a linear system solve for every value of s . In cases where the system dimension n is large and a high resolution is required, i.e., a high number of values of s , the evaluation of the transfer function is very expensive. On the other hand, model order reduction for linear dynamical systems is a technique that approximates a system Σ by another system $\hat{\Sigma}$ of the same form but of a much lower dimension (order) $k \ll n$. Consequently, evaluating the transfer function of $\hat{\Sigma}$ is relatively cheap since it only involves linear system solves of dimension k instead of linear system solves of dimension n for Σ .

Let the system Σ be given by (36) and define a matrix $\mathbf{V} \in \mathbb{R}^{n \times k}$ with orthonormal columns, i.e., $\mathbf{V}^\top\mathbf{V} = \mathbf{I}$. Then, a reduced order model $\hat{\Sigma}$ can be constructed by applying a

Galerkin projection $\mathbf{P} = \mathbf{V}\mathbf{V}^\top$ onto Σ , yielding

$$\widehat{\Sigma} = \begin{cases} (\widehat{\mathbf{H}} - s\widehat{\mathbf{S}})\widehat{\mathbf{x}}(s) = \widehat{\mathbf{b}}u(s) \\ \widehat{\mathbf{y}}(s) = \widehat{\mathbf{c}}^\top\widehat{\mathbf{x}}(s) \end{cases}, \quad (40)$$

where $\widehat{\mathbf{H}} = \mathbf{V}^\top\mathbf{H}\mathbf{V}$, $\widehat{\mathbf{S}} = \mathbf{V}^\top\mathbf{S}\mathbf{V}$, $\widehat{\mathbf{b}} = \mathbf{V}^\top\mathbf{b}$, and $\widehat{\mathbf{c}}^\top = \mathbf{c}^\top\mathbf{V}$. Note that the state vector $\widehat{\mathbf{x}}$ and the dimension of $\widehat{\Sigma}$ is only $k \ll n$. Thus, the aim of model order reduction is to construct a \mathbf{V} such that the transfer function of $\widehat{\Sigma}$ approximates very well the one of Σ ,

$$\gamma_\Sigma(s) \approx \gamma_{\widehat{\Sigma}}(s), \quad (41)$$

for all s we are interested in.

Before explaining how to construct such a \mathbf{V} , we introduce the concept of moments and moment matching. Let the transfer function γ of Σ be given by (37). Then the ℓ th moment of γ around the point $s = s_\star$ is defined as the ℓ th derivative of γ evaluated at s_\star , i.e.,

$$\mathbf{m}_\ell(s_\star) := (-1)^\ell \left. \frac{d^\ell}{ds^\ell} \gamma(s) \right|_{s=s_\star}, \quad (42)$$

for $\ell \geq 0$. Consequently, since $\gamma(s) = \mathbf{c}^\top (\mathbf{H} - s\mathbf{S})^{-1} \mathbf{b}$, the moments at s_\star are

$$\begin{aligned} \mathbf{m}_0(s_\star) &= \mathbf{c}^\top (\mathbf{H} - s_\star\mathbf{S})^{-1} \mathbf{b}, \\ \mathbf{m}_\ell(s_\star) &= \mathbf{c}^\top (\mathbf{H} - s_\star\mathbf{S})^{-(\ell+1)} \mathbf{b}, \quad \ell > 0. \end{aligned}$$

Note also that the moments determine the coefficients of the Taylor series expansion of the transfer function γ in the neighborhood of s_\star

$$\gamma(s) = \mathbf{m}_0(s_\star) + \mathbf{m}_1(s_\star) \frac{s - s_\star}{1!} + \mathbf{m}_2(s_\star) \frac{(s - s_\star)^2}{2!} + \dots \quad (43)$$

Model order reduction via moment matching consists of constructing a subspace $\mathbf{V} \in$

$\mathbb{R}^{n \times km}$ such that the original and reduced order model match moments

$$\mathbf{m}_{i_j}(s_j) = \widehat{\mathbf{m}}_{i_j}(s_j), \quad j = 1, \dots, k. \quad (44)$$

If all moments to be matched are chosen at zero, i.e., $s_j = 0$ for $j = 1, 2, \dots, k$, the corresponding problem is known as Padé approximation. In the general case, the problem (44) is known as rational interpolation and can be solved by choosing the projection matrix \mathbf{V} as follows⁴⁷

$$\mathbf{V} = \text{span} \left[(\mathbf{H} - s_1 \mathbf{S})^{-1} \mathbf{b} \quad (\mathbf{H} - s_2 \mathbf{S})^{-1} \mathbf{b} \quad \dots \quad (\mathbf{H} - s_k \mathbf{S})^{-1} \mathbf{b} \right]. \quad (45)$$

It can be shown that the matrix \mathbf{V} defined in (45) spans a rational Krylov subspace and matches all the 0th moments at s_j . Furthermore, for systems with symmetric \mathbf{H} , symmetric \mathbf{S} , and \mathbf{b} and \mathbf{c} linearly dependent, e.g., the system associated with the absorption spectrum (22), it can be proven that a reduced order model of dimension k matches $2k$ moments instead of only k moments in the general case.

References

- (1) Stöhr, J. *NEXAFS spectroscopy*; Springer Science & Business Media, 2013; Vol. 25.
- (2) Yannoulis, P.; Dudde, R.; Frank, K.; Koch, E. Orientation of Aromatic Hydrocarbons on Metal Surfaces as Determined by NEXAFS. *Surf. Sci.* **1987**, *189*, 519–528.
- (3) Aygül, U.; Batchelor, D.; Dettinger, U.; Yilmaz, S.; Allard, S.; Scherf, U.; Peisert, H.; Chassé, T. Molecular Orientation in Polymer Films for Organic Solar Cells Studied by NEXAFS. *J. Phys. Chem. C* **2012**, *116*, 4870–4874.
- (4) Shadle, S. E.; Hedman, B.; Hodgson, K. O.; Solomon, E. I. Ligand K-Edge X-Ray

- Absorption Spectroscopic Studies. Metal-Ligand Covalency in a Series of Transition Metal Tetrachlorides. *J. Am. Chem. Soc.* **1995**, *117*, 2259–2272.
- (5) DuBois, J. L.; Mukherjee, P.; Stack, T.; Hedman, B.; Solomon, E. I.; Hodgson, K. O. A Systematic K-Edge X-Ray Absorption Spectroscopic Study of Cu (III) Sites. *J. Am. Chem. Soc.* **2000**, *122*, 5775–5787.
- (6) Chen, L. X.; Jäger, W. J.; Jennings, G.; Gosztola, D. J.; Munkholm, A.; Hessler, J. P. Capturing a photoexcited molecular structure through time-domain X-ray absorption fine structure. *Science* **2001**, *292*, 262–264.
- (7) Chen, L. X.; Shelby, M. L.; Lestrangle, P. J.; Jackson, N. E.; Haldrup, K.; Mara, M. W.; Stickrath, A. B.; Zhu, D.; Lemke, H.; Chollet, M.; Hoffman, B. M.; Li, X. Imaging Ultrafast Excited State Pathways in Transition Metal Complexes by X-ray Transient Absorption and Scattering using X-ray Free Electron Laser Source. *Faraday Discuss.* **2016**, *194*, 639–658.
- (8) Shelby, M. L.; Lestrangle, P. J.; Jackson, N. E.; Haldrup, K.; Mara, M. W.; Stickrath, A. B.; Zhu, D.; Lemke, H.; Chollet, M.; Hoffman, B. M.; Li, X.; Chen, L. X. Ultrafast Excited State Relaxation of a Metalloporphyrin Revealed by Femtosecond X-ray Absorption Spectroscopy. *J. Am. Chem. Soc.* **2016**, *138*, 8752–8764.
- (9) Li, X.; Smith, S. M.; Markevitch, A. N.; Romanov, D. A.; Levis, R. J.; Schlegel, H. B. A Time-dependent Hartree-Fock Approach for Studying the Electronic Optical Response of Molecules in Intense Fields. *Phys. Chem. Chem. Phys.* **2005**, *7*, 233–239.
- (10) Li, X.; Tully, J. C. Ab initio Time-resolved Density Functional Theory for Lifetimes of Excited Adsorbate States at Metal Surfaces. *Chem. Phys. Lett.* **2007**, *439*, 199.
- (11) Liang, W.; Chapman, C. T.; Li, X. Efficient First-principles Electronic Dynamics. *J. Chem. Phys.* **2011**, *134*, 184102.

- (12) Lopata, K.; Van Kuiken, B. E.; Khalil, M.; Govind, N. Linear-response and real-time time-dependent density functional theory studies of core-level near-edge x-ray absorption. *J. Chem. Theor. Comput.* **2012**, *8*, 3284–3292.
- (13) Bruner, A.; LaMaster, D.; Lopata, K. Accelerated broadband spectra using transition dipole decomposition and Padé approximants. *J. Chem. Theor. Comput.* **2016**, *12*, 3741–3750.
- (14) Olsen, J.; Jensen, H. J. A.; Jørgensen, P. Solution of the large matrix equations which occur in response theory. *J. Comput. Phys.* **1988**, *74*, 265–282.
- (15) Monkhorst, H. J. Calculation of Properties with the Coupled-Cluster Method. *Int. J. Quant. Chem.* **1977**, *12*, 421–432.
- (16) Koch, H.; Jørgensen, P. Coupled Cluster Response Functions. *J. Chem. Phys.* **1990**, *93*, 3333–3344.
- (17) Stanton, J. F.; Bartlett, R. J. The Equation of Motion Coupled-Cluster Method. A Systematic Biorthogonal Approach to Molecular Excitation Energies, Transition Probabilities, and Excited State Properties. *J. Chem. Phys.* **1993**, *98*, 7029–7039.
- (18) Comeau, D. C.; Bartlett, R. J. The Equation-of-Motion Coupled-Cluster Method. Applications to Open-and Closed-Shell Reference States. *Chem. Phys. Lett.* **1993**, *207*, 414–423.
- (19) Wenzel, J.; Wormit, M.; Dreuw, A. Calculating X-ray absorption spectra of open-shell molecules with the unrestricted algebraic-diagrammatic construction scheme for the polarization propagator. *J. Chem. Theor. Comput.* **2014**, *10*, 4583.
- (20) Wenzel, J.; Wormit, M.; Dreuw, A. Calculating core-level excitations and X-ray absorption spectra of large and medium sized closed-shell molecules with the algebraic-

- diagrammatic construction scheme for the polarization propagator. *J. Chem. Theor. Comput.* **2014**, *35*, 1900.
- (21) Casida, M. E. In *Recent Advances in Density Functional Methods:(Part I)*; Chong, D. P., Ed.; World Scientific; Singapore, 1995; Vol. 1; pp 155–193.
- (22) Dreuw, A.; Head-Gordon, M. Single-Reference Ab Initio Methods for the Calculation of Excited States of Large Molecules. *Chem. Rev.* **2005**, *105*, 4009–4037.
- (23) Helgaker, T.; Coriani, S.; Jørgensen, P.; Kristensen, K.; Olsen, J.; Ruud, K. Recent Advances in Wave Function-Based Methods of Molecular-Property Calculations. *Chem. Rev.* **2012**, *112*, 543–631.
- (24) Shavitt, I.; Bartlett, R. J. *Many-Body Methods in Chemistry and Physics: MBPT and Coupled-Cluster Theory*; Cambridge university press, 2009.
- (25) Liang, W.; Fischer, S. A.; Frisch, M. J.; Li, X. Energy-Specific Linear Response TDHF/TDDFT for Calculating High-Energy Excited States. *J. Chem. Theor. Comput.* **2011**, *7*, 3540–3547.
- (26) Lestrangle, P. J.; Nguyen, P. D.; Li, X. Calibration of Energy-Specific TDDFT for Modeling K-edge XAS Spectra of Light Elements. *J. Chem. Theor. Comput.* **2015**, *11*, 2994–2999.
- (27) Peng, B.; Lestrangle, P. J.; Goings, J. J.; Caricato, M.; Li, X. Energy-Specific Equation-of-Motion Coupled-Cluster Methods for High-Energy Excited States: Application to K-edge X-ray Absorption Spectroscopy. *J. Chem. Theor. Comput.* **2015**, *11*, 4146–4153.
- (28) Stener, M.; Fronzoni, G.; De Simone, M. Time Dependent Density Functional Theory of Core Electrons Excitations. *Chem. Phys. Lett.* **2003**, *373*, 115–123.
- (29) Ray, K.; DeBeer George, S.; Solomon, E. I.; Wieghardt, K.; Neese, F. Description of the Ground-State Covalencies of the Bis (dithiolato) Transition-Metal Complexes from

- X-ray Absorption Spectroscopy and Time-Dependent Density-Functional Calculations. *Chem. Eur. J.* **2007**, *13*, 2783–2797.
- (30) Besley, N. A.; Asmuruf, F. A. Time-Dependent Density Functional Theory Calculations of the Spectroscopy of Core Electrons. *Phys. Chem. Chem. Phys.* **2010**, *12*, 12024–12039.
- (31) Davidson, E. R. The Iterative Calculation of a Few of the Lowest Eigenvalues and Corresponding Eigenvectors of Large Real-Symmetric Matrices. *J. Comput. Phys.* **1975**, *17*, 87.
- (32) Morgan, R. B.; Scott, D. S. Generalizations of Davidson’s Method for Computing Eigenvalues of Sparse Symmetric Matrices. *SIAM J. Sci. Statist. Comput.* **1986**, *7*, 817–825.
- (33) Morgan, R. B. Generalizations of Davidson’s Method for Computing Eigenvalues of Large Non-Symmetric Matrices. *J. Comput. Phys.* **1992**, *101*, 287–291.
- (34) Zuev, D.; Vecharynski, E.; Yang, C.; Orms, A. I., Natalie abd Krylov New Algorithms for Iterative Matrix-Free Eigensolvers in Quantum Chemistry. *J. Comput. Chem.* **2015**, *36*, 273–284.
- (35) Christiansen, O.; Jørgensen, P.; Hättig, C. Response Functions from Fourier Component Variational Perturbation Theory Applied to a Time-Averaged Quasienergy. *Int. J. Quant. Chem.* **1998**, *68*, 1–52.
- (36) Kauczor, J.; Jørgensen, P.; Norman, P. On the Efficiency of Algorithms for Solving Hartree-Fock and Kohn-Sham Response Equations. *J. Chem. Theor. Comput.* **2011**, *7*, 1610–1630.
- (37) Coriani, S.; Fransson, T.; Christiansen, O.; Norman, P. Asymmetric-Lanczos-chain-driven implementation of electronic resonance convergent coupled-cluster linear response theory. *J. Chem. Theor. Comput.* **2012**, *8*, 1616–1628.

- (38) Fransson, T.; Coriani, S.; Christiansen, O.; Norman, P. Carbon X-ray Absorption Spectra of Fluoroethenes and Acetone: A Study at the Coupled Cluster, Density Functional, and Static-exchange Levels of Theory. *J. Chem. Phys.* **2013**, *138*, 124311.
- (39) Kauczor, J.; Norman, P.; Christiansen, O.; Coriani, S. Communication: A Reduced-Space Algorithm for the Solution of the Complex Linear Response Equations used in Coupled Cluster Damped Response Theory. 2013.
- (40) Marques, M. A.; Maitra, N. T.; Nogueira, F. M.; Gross, E. K.; Rubio, A. *Fundamentals of Time-Dependent Density Functional Theory*; Springer Science & Business Media, 2012; Vol. 837; Chapter 7.
- (41) Fahleson, T.; Ågren, H.; Norman, P. A Polarization Propagator for Nonlinear X-ray Spectroscopies. *J. Phys. Chem. Lett.* **2016**, *7*, 1991–1995.
- (42) Coriani, S.; Christiansen, O.; Fransson, T.; Norman, P. Coupled-Cluster Response Theory for Near-Edge X-Ray-Absorption Fine Structure of Atoms and Molecules. *Phys. Rev. A* **2012**, *85*, 022507.
- (43) Linares, M.; StafstroÛm, S.; Rinkevicius, Z.; Ågren, H.; Norman, P. Complex Polarization Propagator Approach in the Restricted Open-Shell, Self-Consistent Field Approximation: The Near K-Edge X-ray Absorption Fine Structure Spectra of Allyl and Copper Phthalocyanine. *J. Phys. Chem. B* **2010**, *115*, 5096–5102.
- (44) Ekström, U.; Norman, P.; Carravetta, V.; Ågren, H. Polarization Propagator for X-ray Spectra. *Phys. Rev. Lett.* **2006**, *97*, 143001.
- (45) Villaume, S.; Saue, T.; Norman, P. Linear Complex Polarization Propagator in a Four-Component Kohn–Sham Framework. *J. Chem. Phys.* **2010**, *133*, 064105.
- (46) Fransson, T.; Burdakova, D.; Norman, P. K- and L-Edge X-Ray Absorption Spectrum Calculations of Closed-Shell Carbon, Silicon, Germanium, and Sulfur Compounds using

- Damped Four-Component Density Functional Response Theory. *Phys. Chem. Chem. Phys.* **2016**, *18*, 13591–13603.
- (47) Antoulas, A. C. In *Advances in Design and Control 6*; Ralph C. Smith North Carolina State University, Ed.; Advances in Design and Control 6; SIAM, 2005; p 479.
- (48) Oddershede, J.; Jørgensen, P.; Yeager, D. L. Polarization Propagator Methods in Atomic and Molecular Calculations. *Comp. Phys. Rep.* **1984**, *2*, 33–92.
- (49) Benner, P.; Mehrmann, V.; Xu, H. A numerically stable, structure preserving method for computing the eigenvalues of real Hamiltonian or symplectic pencils. *Numer. Math.* **1998**, *78*, 329–358.
- (50) Bai, Z.; Li, R.-C. Minimization principles for the linear response eigenvalue problem I: Theory. *SIAM J. Mat. Anal. Appl.* **2012**, *33*, 1075–1100.
- (51) Shao, M.; da Jornada, F. H.; Yang, C.; Deslippe, J.; Louie, S. G. Structure preserving parallel algorithms for solving the Bethe–Salpeter eigenvalue problem. *Linear Algebra Appl.* **2016**, *488*, 148–167.
- (52) Stratmann, R. E.; Scuseria, G. E.; Frisch, M. J. An Efficient Implementation of Time-Dependent Density-Functional Theory for the Calculation of Excitation Energies of Large Molecules. *J. Chem. Phys.* **1998**, *109*, 8218–8224.
- (53) Brabec, J.; Lin, L.; Shao, M.; Govind, N.; Yang, C.; Saad, Y.; Ng, E. G. Efficient Algorithms for Estimating the Absorption Spectrum within Linear Response TDDFT. *J. Chem. Theor. Comput.* *11*, 5197–5208.
- (54) Li, X.; Valeev, E. F.; Williams-Young, D.; Ding, F.; Liu, H.; Goings, J.; Petrone, A.; Lestrange, P. Chronus Quantum, Beta Version. 2017; <http://www.chronusquantum.org>.

- (55) Walker, H. F. Implementation of the GMRES Method using Householder Transformations. *SIAM J. Sci. Stat. Comp.* **1988**, *9*, 152–163.
- (56) Shao, M.; Aktulga, H. M.; Yang, C.; Ng, E. G.; Maris, P.; Vary, J. P. Accelerating Nuclear Configuration Interaction Calculations through a Preconditioned Block Iterative Eigensolver. *arXiv* **2016**, *abs/1609.01689*.
- (57) McLachlan, A.; Ball, M. Time-Dependent Hartree–Fock Theory for Molecules. *Rev. Mod. Phys.* **1964**, *36*, 844.
- (58) Harris, R. A. Oscillator Strengths and Rotational Strengths in Hartree–Fock Theory. *J. Chem. Phys.* **1969**, *50*, 3947–3951.
- (59) Yeager, D.; Nascimento, M.; McKoy, V. Some Applications of Excited-State-Excited-State Transition Densities. *Phys. Rev. A* **1975**, *11*, 1168.